



**British  
Geological Survey**

NATURAL ENVIRONMENT RESEARCH COUNCIL

# Mineralogical, geochemical and petrographical characterisation of Nordland Shale cores from well 15/9-A-11, Sleipner field, northern North Sea

Sustainable Energy and Geophysical Surveys Programme

Commissioned Report CR/02/313





BRITISH GEOLOGICAL SURVEY

COMMISSIONED REPORT CR/02/313

# Mineralogical, geochemical and petrographical characterisation of Nordland Shale cores from well 15/9-A-11, Sleipner field, northern North Sea

S J Kemp, J M Pearce and E J Steadman

The National Grid and other Ordnance Survey data are used with the permission of the Controller of Her Majesty's Stationery Office.  
Ordnance Survey licence number GD 272191/1999

*Key words*

CO<sub>2</sub> storage, Sleipner, North Sea, mineralogy, petrography, cap rock, clay minerals.

*Front cover*

Scanning electron photomicrograph of a detrital and compactionally deformed chlorite flake being replaced by kaolinite. Core 2 (907.55 - 907.60 m).

*Bibliographical reference*

KEMP, S J, PEARCE, J M and STEADMAN, E J. 2002. Mineralogical, geochemical and petrographical characterisation of Nordland Shale cores from well 15/9-A-11, Sleipner field, northern North Sea. *British Geological Survey Commissioned Report*, CR/02/313. 40pp.

## BRITISH GEOLOGICAL SURVEY

The full range of Survey publications is available from the BGS Sales Desks at Nottingham and Edinburgh; see contact details below or shop online at [www.thebgs.co.uk](http://www.thebgs.co.uk)

The London Information Office maintains a reference collection of BGS publications including maps for consultation.

The Survey publishes an annual catalogue of its maps and other publications; this catalogue is available from any of the BGS Sales Desks.

*The British Geological Survey carries out the geological survey of Great Britain and Northern Ireland (the latter as an agency service for the government of Northern Ireland), and of the surrounding continental shelf, as well as its basic research projects. It also undertakes programmes of British technical aid in geology in developing countries as arranged by the Department for International Development and other agencies.*

*The British Geological Survey is a component body of the Natural Environment Research Council.*

### Keyworth, Nottingham NG12 5GG

☎ 0115-936 3241 Fax 0115-936 3488  
e-mail: [sales@bgs.ac.uk](mailto:sales@bgs.ac.uk)  
[www.bgs.ac.uk](http://www.bgs.ac.uk)  
Shop online at: [www.thebgs.co.uk](http://www.thebgs.co.uk)

### Murchison House, West Mains Road, Edinburgh EH9 3LA

☎ 0131-667 1000 Fax 0131-668 2683  
e-mail: [scotsales@bgs.ac.uk](mailto:scotsales@bgs.ac.uk)

### London Information Office at the Natural History Museum (Earth Galleries), Exhibition Road, South Kensington, London SW7 2DE

☎ 020-7589 4090 Fax 020-7584 8270  
☎ 020-7942 5344/45 email: [bgs london@bgs.ac.uk](mailto:bgs london@bgs.ac.uk)

### Forde House, Park Five Business Centre, Harrier Way, Sowton, Exeter, Devon EX2 7HU

☎ 01392-445271 Fax 01392-445371

### Geological Survey of Northern Ireland, 20 College Gardens, Belfast BT9 6BS

☎ 028-9066 6595 Fax 028-9066 2835

### Macleans Building, Crowmarsh Gifford, Wallingford, Oxfordshire OX10 8BB

☎ 01491-838800 Fax 01491-692345

### Parent Body

### Natural Environment Research Council, Polaris House, North Star Avenue, Swindon, Wiltshire SN2 1EU

☎ 01793-411500 Fax 01793-411501  
[www.nerc.ac.uk](http://www.nerc.ac.uk)

## Foreword

This report is the published product of a study by the British Geological Survey (BGS) and forms part of the international SACS (Saline Aquifer CO<sub>2</sub> Storage) project. The project aims to monitor and predict the behaviour of injected CO<sub>2</sub> in the Utsira Sand reservoir at the Sleipner field in the northern North Sea by methods including time-lapse geophysics, modelling its subsurface distribution and migration, and simulating likely chemical interactions with the host rock.

This report provides mineralogical, geochemical and petrographical data for three mudstone core samples to help characterise and predict the sealing capacity of the Nordland Shale cap rock overlying the Utsira Sand reservoir.

## Acknowledgements

The authors wish to acknowledge the following BGS colleagues for their efforts in producing this report: B Vickers for CEC analysis, G Turner for SEM preparation, D Oates for PTS preparation, J Cook and XRFS staff for geochemical analysis.

# Contents

<b>Foreword</b> .....	<b>i</b>
<b>Acknowledgements</b> .....	<b>i</b>
<b>Contents</b> .....	<b>ii</b>
<b>Summary</b> .....	<b>v</b>
<b>1 Introduction</b> .....	<b>1</b>
<b>2 Samples</b> .....	<b>1</b>
<b>3 Laboratory methods</b> .....	<b>2</b>
3.1 General sample preparation .....	2
3.2 Particle-size analysis .....	2
3.3 X-ray diffraction analysis .....	2
3.4 Geochemistry .....	3
3.5 Surface area determinations .....	4
3.6 Cation exchange capacity .....	4
3.7 Total organic carbon analysis .....	4
3.8 Petrographic analysis .....	4
<b>4 Results</b> .....	<b>5</b>
4.1 Particle-size analysis .....	5
4.2 X-ray diffraction analysis .....	6
4.3 Geochemistry .....	7
4.4 Surface area and cation exchange capacity determinations .....	8
4.5 Total organic carbon analysis .....	8
4.6 Petrographic analysis .....	8
<b>5 Discussion</b> .....	<b>10</b>
5.1 Comparison with previous studies .....	10
5.2 Seal capacity prediction .....	11
<b>6 Conclusions</b> .....	<b>13</b>
<b>References</b> .....	<b>14</b>
<b>Appendix - X-ray diffraction traces</b> .....	<b>27</b>

## TABLES

Table 1. Samples .....	2
Table 2. Summary of particle-size analysis and classification .....	5
Table 3. Summary of quantitative whole-rock X-ray diffraction analysis .....	6
Table 4. Summary of quantitative <2 $\mu\text{m}$ fraction X-ray diffraction analysis .....	6
Table 5. Summary of geochemistry by X-ray fluorescence spectroscopy .....	7
Table 6. Summary of geochemistry by ICP-MS. ....	7
Table 7. Summary of surface area, CEC and TOC determinations .....	8

## FIGURES

Figure 1. Northern and Central North Sea map showing location of the Sleipner field. ....	15
Figure 2. BGS sampling strategy for the four Sleipner caprock cores .....	16
Figure 3. Core 1, 906.13 – 906.20 m, end-view prior to liner removal (above), side-view following liner removal (below). ....	17
Figure 4. Core 2, 907.55 – 907.60 m, end-view prior to liner removal (above), side-view following liner removal (below). ....	18
Figure 5. Core 4, 910.22 – 910.30 m, end-view prior to liner removal (above), side-view following liner removal (below). ....	19
Figure 6. Cumulative plot of particle-size data. ....	20
Figure 7. Triangular plot of particle-size data (after Shepard, 1954) .....	20
Figure 8. Scanning electron photomicrographs of spherical granules produced by spray-drying to ensure a random arrangement of component particles for whole-rock XRD analysis, sample Core 1, 906.13 – 906.20 m. ....	21
Figure 9. Geochemistry of the core samples, XRF major elements (upper chart), selected XRF trace elements (middle chart) and ICP-MS trace elements (lower chart). ....	22
Figure 10. Geochemical distributions for the core samples compared to the North American Shale Composite (Gromet <i>et al.</i> , 1984). ....	23
Figure 11. Typical, weakly laminated, moderately compacted silty mudstone comprising medium-sized subangular silt grains in a clay matrix. Core 1 (906.13 – 906.20 m). H973P101.tif. ....	24
Figure 12. Detailed view of typical moderately compacted clay fabric with very fine detrital silt grains and authigenic ankerite (a) occurring throughout. Core 1 (906.13 – 906.20 m). H973P102.tif. ....	24
Figure 13. A detrital, altered muscovite grain with ankerite (a) and pyrite (p) infilling secondary porosity along basal cleavages. Note moderate compaction and mica alignment around coarser silt grains. Core 1 (906.13 – 906.20 m). H973P104.tif. ....	24
Figure 14. Typical view of silty mudstone from Core 2 (907.55 – 907.60 m). Note irregular silt grains, and partially replaced phyllosilicates. H974P106.tif. ....	24
Figure 15. A biotite grain which is altering and splaying along basal cleavages, within which REE-phosphates (REE) are precipitating. Note rare authigenic REE-phosphate (REE) close-by in the matrix. Core 2 (907.55 – 907.60 m). H974P101.tif. ....	24

**FIGURES (continued)**

- Figure 16. A rare, severely altered chlorite (c) with ankerite (a) and pyrite (p) precipitating in resultant secondary porosity. Core 2 (907.55 – 907.60 m). H974P107.tif. ....24
- Figure 17. A detrital and compactionally deformed chlorite flake that is being replaced by kaolinite. Core 2 (907.55 – 907.60 m). H974P102.tif. ....25
- Figure 18. A close-up of the altered chlorite (c) in Figure 13, being replaced by kaolinite (k). Core 2 (907.55 – 907.60 m). H974P103.tif. ....25
- Figure 19. Framboidal pyrite aggregates forming millimetre-scale lenses. Core 2 (907.55 – 907.60 m). H974P108.tif. ....25
- Figure 20. Typical view of moderately compacted silty mudstone with lamination defined by parallel oriented detrital phyllosilicates, from Core 4 (910.26 – 910.30 m). H975P102.tif. 25
- Figure 21. Detailed view of domainal orientations, identified by dashed boundaries, in the clay matrix. Core 4 (910.26 – 910.30 m). H975P103.tif. ....25
- Figure 22. A silt grain plucked during specimen preparation reveals pore-throats blocked by detrital and authigenic illitic clay flakes (i). Core 4 (910.26 – 910.30 m). H975S101.tif. ....25

## Summary

This report summarises the results of mineralogical, geochemical and petrographical characterisation of three mudstone core samples (Nordland Shale) taken from well 15/9-A-11, northern North Sea. A range of analyses including X-ray diffraction, X-ray fluorescence, inductively coupled plasma-mass spectroscopy, scanning electron microscopy, particle-size analysis, cation exchange capacity and total organic carbon analyses were employed in order to fully characterise the samples. The results of such analyses were then used to predict the seal capacity of the Nordland Shale for injected CO<sub>2</sub> in the underlying Utsira Sand reservoir.

The fine-grained clay or silty clay samples show broadly similar characteristics to previously studied material and are composed of undifferentiated mica, quartz, kaolinite, K-feldspar, calcite, smectite, albite, chlorite, pyrite and halite. The cores have a weak, sedimentary lamination and lack primary and secondary porosity.

The samples have similar geochemistries which closely match that of the North American Shale Composite (NASC). Geochemical variations can generally be explained in terms of the detected mineralogy with the exception of Fe<sub>2</sub>O<sub>3t</sub> which may suggest the undetected presence of poorly crystalline Fe-oxyhydroxides.

Although small quantities of smectite in the Nordland Shale may invalidate its predictions, XRD-determined quartz contents suggest displacement pore throat diameters of 2.2 to 21.1 nm using the Krushin (1997) methodology. As found by previous workers, considering that the Utsira Sand has a maximum thickness of *c.* 300 m in the Sleipner area, capillary leakage through the Nordland Shale would appear unlikely.



# 1 Introduction

Due to the global warming threat posed by anthropogenic greenhouse gases there is an urgent need to develop ways of lowering industrial CO<sub>2</sub> emissions. The world's first geological CO<sub>2</sub> sequestration operation is currently running at the Sleipner field in the northern North Sea. Here, CO<sub>2</sub> is being injected into the Mio-Pliocene Utsira Sand, a subsurface saline aquifer, at a depth of about 1000 m below sea level. The injected CO<sub>2</sub> then migrates upwards but is trapped by the overlying, shale-dominated Nordland Group. The operation commenced in 1996, and is expected to last for 20 years, injecting at an average rate of about one million tonnes per year.

The British Geological Survey (BGS) is part of the international SACS (Saline Aquifer CO<sub>2</sub> Storage) project, whose aims include monitoring the injected CO<sub>2</sub> by time-lapse geophysical methods, modelling its subsurface distribution and migration, and simulating likely chemical interactions with the host rock.

As part of this study, this report describes the mineralogical characterisation of samples of the Nordland Shale, the cap rock sequence taken from *c.* 100 m above the Utsira Sand (A. Chadwick, *pers. comm.*), northern North Sea. A location map of the Northern and Central North Sea is shown in Figure 1 to indicate the position of the Utsira Sand and Sleipner field. Prior to the SACS program, characterisation of the Nordland Shale was limited to interpretation of seismic data, wire-line logs and the macroscopic description of cuttings. As part of the SACS program, Lothe & Zweigel (1999) and Bøe & Zweigel (2000) provided quantitative mineralogical descriptions of samples from Norwegian Block 15/9 using X-ray diffraction and petrographic analyses. Kemp *et al.* (2001), presented mineralogical and petrographic data, augmented by further analytical techniques, for samples from UK Quadrant 16, to the west of the Sleipner area.

By employing the empirical relationships suggested by Krushin (1997), such mineralogical data can be used to determine the maximum CO<sub>2</sub> column required to cause capillary failure in the cap rock seal. This data could then be compared with laboratory experiments also carried out on the core and designed to directly measure such parameters.

The geological framework of the area was summarised by Bøe & Zweigel (2000). In summary, the cap rock sequence for the Utsira Sand varies between 200 and 300 m in thickness in the Sleipner area which can be divided into three main units on the basis of seismic character. The most important of these for the present study is the lowest Upper Pliocene unit or 'shale drape', a *c.* 50 to 100 m thick sequence which directly overlies the Utsira Sand. Sand and silt stringers occur towards the base of the middle unit, close to the basin margins (Chadwick *et al.*, 2000).

## 2 Samples

Four core samples were supplied to the BGS by Statoil in July 2002 for various testing procedures. After opening the cores, subsamples for mineralogical, geochemical and petrographical characterisation were cut following the scheme shown in Figure 2 and listed in Table 1. Photographs of the core samples are shown in Figures 3-5.

The subsamples for mineralogical, geochemical and petrographical characterisation were longitudinally sliced into three approximately equal parts. After removal of its ?contaminated rind, one third was dried overnight at 55°C for mineralogical and geochemical characterisation (X-ray diffraction, (XRD) analysis, surface area and cation exchange determinations (CEC), total organic carbon (TOC), particle-size analysis and geochemistry by X-ray fluorescence (XRF) and inductively coupled plasma-mass spectroscopy (ICP-MS)). A second third was used for petrographical analysis while the remaining third was kept refrigerated as reference material.

**Table 1. Samples**

Core no.	Depth (m)			BGS mineralogy lab. code	Description
	Top	Bottom	Mean		
1	906.13	906.20	906.17	MPLH973	Grey-green, firm, laminated mudstone
2	907.55	907.60	907.58	MPLH974	Grey-green, firm, laminated mudstone
4	910.26	910.30	910.28	MPLH975	Grey-green, firm, laminated mudstone

## 3 Laboratory methods

### 3.1 GENERAL SAMPLE PREPARATION

The dried material for mineralogical and geochemical characterisation was initially jaw-crushed. Half of this crushed material was then subsampled and hammer-milled to <0.12 mm for whole-rock XRD analysis, TOC analysis and CEC determinations. A subsample of the crushed material was agate tema –milled for geochemical analysis.

### 3.2 PARTICLE-SIZE ANALYSIS

Approximately 12 g jaw-crushed material was dispersed in deionised water using a laboratory shaker and treatment with ultrasound. The dispersed material was then wet screened on a 63  $\mu\text{m}$  aperture sieve, and the >63  $\mu\text{m}$  material was dried at 55°C and weighed. The <63  $\mu\text{m}$  material was then divided into two portions – one for further particle-size analysis and the other for clay mineral X-ray diffraction analysis (see Section 3.3).

Analysis of the material <63  $\mu\text{m}$  was carried out using a 0.05% ‘Calgon’ (sodium hexametaphosphate) solution in a Micromeritics Sedigraph 5100 particle-size analyser. The results of Sedigraph analysis are similar to those obtained by Andreasen pipette (stipulated by BS1377: 1190) as both are sedimentation methods utilizing Stokes’ Law.

### 3.3 X-RAY DIFFRACTION ANALYSIS

#### 3.3.1 Whole-rock analysis

In order to produce a finer and uniform particle-size for whole-rock XRD analysis, a portion of the hammer-milled material was micronised under deionised water for 10 minutes and then spray-dried using the method outlined in Hillier (1999). The spray-dried material, in the form of *c.*40  $\mu\text{m}$  diameter spheres of randomly oriented particles helps reduce preferred orientation effects that are one of the largest sources of error in quantitative XRD analysis. The spray-dried material was front-loaded into a standard aluminium sample holder.

XRD analyses were carried out using a Philips PW1700 series automatic diffractometer equipped with a cobalt target X-ray tube and operating at 45 kV and 40 mA. Diffraction data were analysed using Philips X’Pert software coupled to an International Centre for Diffraction Data (ICDD) database running on a Gateway personal computer system. The whole-rock samples were scanned from 3-50  $^{\circ}2\theta$  at a scanning speed of 0.48  $^{\circ}2\theta/\text{minute}$ .

Following identification of the mineral species present in the samples, whole-rock mineral quantification was achieved using the Rietveld refinement technique (e.g. Snyder and Bish,

1989) using Siroquant v.2.5 software. This method avoids the need to produce synthetic mixtures and involves the least squares fitting of measured to calculated XRD profiles using a crystal structure databank.

Errors for the quoted mineral concentrations are typically  $\pm 2.5\%$  for concentrations  $>60$  wt%,  $\pm 5\%$  for concentrations between 60 and 30 wt%,  $\pm 10\%$  for concentrations between 30 and 10 wt%,  $\pm 20\%$  for concentrations between 10 and 3 wt% and  $\pm 40\%$  for concentrations  $<3$  wt% (Hillier *et al.*, 2001).

### 3.3.2 Clay mineral analysis

In order to determine the nature of any clay minerals present in the samples, *c.* half of the  $<63$   $\mu\text{m}$  material produced during particle-size analysis was placed in a 250 ml measuring cylinder with 0.5 ml 0.1M sodium hexametaphosphate ('Calgon') solution to disperse the individual clay particles and prevent flocculation.

After standing for a period determined from Stokes' Law, a nominal  $<2$   $\mu\text{m}$  fraction was removed and dried at  $55^\circ\text{C}$ . 100 mg of the dried  $<2$   $\mu\text{m}$  material was then re-dispersed in 2 ml deionised water using an ultrasonic bath and pipetted onto a ceramic tile in a vacuum apparatus to produce an oriented mount. The mounts were Ca-saturated using 2 ml of 1M  $\text{CaCl}_2 \cdot 6\text{H}_2\text{O}$  solution, washed twice to remove excess reagent before being allowed to dry at room temperature. Further K-saturated mounts were prepared to distinguish the presence of vermiculite from chlorite. These were similarly prepared using 2 ml of 1M KCl.

The oriented Ca-mounts were scanned from  $2-32$   $^\circ 2\theta$  also at  $0.48$   $^\circ 2\theta/\text{minute}$  after air-drying, ethylene glycol-solvation and heating to  $550^\circ\text{C}$  for 2 hours. Ethylene glycol-solvation was achieved by placing the samples in a desiccator filled with the reagent and heating to  $55^\circ\text{C}$  overnight. K-saturated mounts were scanned using similar settings after air-drying and heating to  $300^\circ\text{C}$  for 2 hours.

In order to assess the relative proportions of any clay minerals present in the samples, modelling of their XRD profiles was carried out using Newmod-for-Windows™ (Reynolds & Reynolds, 1996) software. The modelling process requires the input of diffractometer, scan parameters and a quartz intensity factor (instrumental conditions) and the selection of different clay mineral sheet compositions and chemistries. In addition, an estimate of the crystallite size distribution of the species may be determined by comparing peak profiles of calculated diffraction profiles with experimental data. By modelling the individual clay mineral species in this way, *mineral reference intensities* were established and used for quantitative standardization following the method outlined in Moore and Reynolds (1997).

## 3.4 GEOCHEMISTRY

### 3.4.1 X-ray fluorescence analysis

XRF analysis was carried out using sequential, fully automatic wavelength-dispersive spectrometers (2 x Philips PW2400 and 1 x Philips PW2440) controlled via PCs running SuperQ (version 3.0H) XRF application package.

Pressed powder pellets were prepared for trace element analysis using a binder composed of 9 parts EMU120FD, a styrene copolymer, and 1 part Ceridust 3620, a micronised polyethylene wax. Fused beads for major element analysis were prepared by fusing 0.9 g sample plus 9.0 g flux (66/34  $\text{Li}_2\text{B}_4\text{O}_7$  and  $\text{LiBO}_2$ ) at  $1200^\circ\text{C}$ . Loss on ignition (LOI) was determined on *c.* 1 g sample heated at  $1050^\circ\text{C}$  for one hour.

### 3.4.2 Inductively coupled plasma-mass spectroscopy

Samples for ICP-MS were first digested using a mixture of hydrofluoric, nitric and perchloric acids on an automated hot block. Following filtration and fusion, samples were analysed using a VG ExCell ICP-MS in conjunction with a Cetac ASX-510 autosampler. The system was controlled by a personal computer through dedicated ICP-MS software. The ICP RF forward power was 1350 W and coolant, auxiliary and injector gas flow rates were 13, 0.8 and 0.99 l min<sup>-1</sup> respectively. Data were acquired in peak jumping mode using three 1 minute integrations.

### 3.5 SURFACE AREA DETERMINATIONS

Surface area determinations were performed using the 2-ethoxyethanol (ethylene glycol monoethyl ether, EGME) technique (Carter *et al.*, 1965). The method is based on the formation of a monolayer of EGME molecules on the clay surface under vacuum. Aluminium dishes containing approximately 1.1 g sample/clay standard (Patterson Court Blue bentonite) were placed in a desiccator containing anhydrous phosphorus pentoxide. The desiccator was evacuated and allowed to stand overnight before the dishes were reweighed. The samples were then saturated with 2-ethoxyethanol and placed in a second desiccator containing dry calcium chloride. After 1½ hours, the desiccator was evacuated and left overnight. The sample was then rapidly re-weighed and the weight of 2-ethoxyethanol absorbed determined and the surface area calculated. Finally, a correction based on the Patterson Court Blue standard was applied.

Smectite has a surface area of c.800 m<sup>2</sup>/g while other clay minerals and quartz have surface areas typically less than 100 m<sup>2</sup>/g and 1 m<sup>2</sup>/g respectively. Such a difference in value means that the surface area of a sample can provide a useful estimate of its smectite content.

### 3.6 CATION EXCHANGE CAPACITY

Cation exchange capacity (CEC) determinations were carried out using hammer-milled material and the normal BaCl<sub>2</sub>/triethanolamine titration method. BGS experience has shown that this modified method appears to give a slightly increased CEC value. Data for standard materials analysed with the samples indicates that values might be increased by 10%.

### 3.7 TOTAL ORGANIC CARBON ANALYSIS

Total organic carbon (TOC) analyses were carried out by ALcontrol Geochem Ltd, Chester on 5 g portions of hammer-milled material. The samples were previously treated to obtain material containing only organic carbon compounds and then heated in a flow of oxygen in a Leco CS444 carbon/sulphur analyser. Any carbon present in the samples was therefore converted to carbon dioxide which was measured by an infra-red detector. The percentage carbon was then calculated with respect to the original sample weight.

### 3.8 PETROGRAPHIC ANALYSIS

Scanning electron microscope (SEM) analysis was conducted in order to assess micro-fabrics within the mudrocks, and to identify the mineralogical composition of the silt and sand-grade particles. In addition, attention was paid to the presence/absence of contaminant phases.

Small rock fragments were mounted on Al pin-type SEM stubs and carbon coated. Observations were made using a LEO 435VP variable pressure digital SEM with an Oxford Instruments ISIS300 digital energy dispersive X-ray microanalysis (EDXA) system. An accelerating voltage of 20kV was used, and qualitative EDXA spectra were acquired to aid mineral identification based on their chemical characteristics. Images were recorded digitally.

Samples for polished thin section preparation were resin-impregnated with an epoxy resin, containing a blue dye to aid porosity identification. Once cut and polished, specimens were coated in a thin layer of carbon and examined in the SEM using a solid-state backscatter detector to assess rock fabric. Images were again recorded digitally.

## 4 Results

### 4.1 PARTICLE-SIZE ANALYSIS

The results of the particle-size analyses are summarised in Table 2 and shown as cumulative frequency plots (Figure 6) following the BGS classification (Hallsworth and Knox, 1999).

**Table 2. Summary of particle-size analysis and classification**

Particle-size		Cumulative % finer than		
		Core No. 1	Core No. 2	Core No. 4
$\mu\text{m}$	Phi	906.17 m	907.58 m	910.28 m
125	3.0	100.0	100.0	100.0
63	4.0	99.7	96.3	94.8
60	4.1	99.5	96.0	94.8
50	4.3	99.5	95.4	94.2
40	4.6	99.2	94.1	93.1
30	5.1	99.2	91.9	90.9
25	5.3	98.9	90.6	89.2
20	5.6	98.3	88.6	87.5
15	6.1	96.9	85.5	84.9
10	6.6	95.1	81.5	80.7
8	7.0	93.5	79.1	78.0
6	7.4	90.8	75.5	73.9
5	7.6	88.6	72.5	70.6
4	8.0	85.4	68.3	66.0
3	8.4	80.9	63.1	60.6
2	9.0	73.9	55.4	54.1
1.5	9.4	68.4	50.8	49.5
1	10.0	60.3	44.2	42.2
0.9	10.1	58.2	42.1	40.4
0.8	10.3	55.9	39.3	38.5
0.7	10.5	53.1	36.0	36.3
0.6	10.7	49.8	31.8	33.7
0.5	11.0	45.8	26.7	30.4
0.4	11.3	40.6	20.5	25.8
0.3	11.7	33.8	13.3	19.8
0.2	12.3	24.8	6.1	12.5
0.1	13.3	24.3	4.9	11.1
%sand (>32 $\mu\text{m}$ )		0.8	8.1	9.1
%silt (4-32 $\mu\text{m}$ )		13.8	23.6	24.9
%clay (<4 $\mu\text{m}$ )		85.4	68.3	66.0
Classification (Shepard, 1954)		Clay	Silty clay	Silty clay

The fine-grained nature of the samples is shown by the fact that 85.4, 68.3 and 66.0% material falls within the clay-grade (<4  $\mu\text{m}$ , >8 $\phi$ ) for Core 1, 2 and 4 respectively. The shallowest sample

(Core 1) plots within the clay field while the two deeper samples (Cores 2 and 4) plot within the silty clay field on the triangular plot defined by Shepard (1954) and illustrated in Figure 7.

#### 4.2 X-RAY DIFFRACTION ANALYSIS

The results of quantitative whole-rock and <2  $\mu\text{m}$  fraction XRD analysis are summarised in Tables 3 and 4. Labelled whole-rock and <2  $\mu\text{m}$  fraction XRD charts are reproduced in the Appendix.

**Table 3. Summary of quantitative whole-rock X-ray diffraction analysis**

Core No.	Mean depth (m)	%mineral										
		quartz	K-feldspar	albite	calcite	'mica'	kaolin	smectite	chlorite	pyrite	halite	sylvite
1	906.17	16.2	4.0	4.9	1.6	60.3	9.7	<0.5	<0.5	1.0	1.2	0.9
2	907.58	31.4	6.8	8.8	<0.5	42.5	8.3	1.0	<0.5	<0.5	<0.5	nd
4	910.28	29.7	6.6	8.0	3.8	41.9	6.0	1.9	<0.5	1.3	0.6	nd

'mica' = undifferentiated mica species including muscovite, biotite, illite and illite/smectite etc  
'kaolin' = one of the kaolin group minerals including halloysite, kaolinite etc.

SEM examination of the spray-dried samples show the successful production of *c.*10-50  $\mu\text{m}$  diameter spheres of randomly-oriented particles (Figure 8).

The core samples are principally composed of 'mica' (undifferentiated mica species possibly including muscovite, biotite, illite and illite/smectite etc) and quartz with minor feldspar (K-feldspar and albite), kaolin and traces of calcite, smectite, chlorite, pyrite and halite. Traces of sylvite (KCl) were also identified in Core 1.

In order to provide quantitative clay mineralogical data, peak integration was performed on the illite 001 (*c.*10Å), kaolinite 002 (3.58Å), chlorite 004 (3.54 Å), and smectite 001 (*c.*17Å) reflections. Sample peak areas were then compared with those derived from modelling the individual clay mineral species with Newmod-for-Windows™ and clay concentrations produced.

**Table 4. Summary of quantitative <2  $\mu\text{m}$  fraction X-ray diffraction analysis**

Core No.	Mean depth (m)	%clay mineral			
		smectite	illite	chlorite	kaolinite
1	906.17	2	60	10	28
2	907.58	7	48	10	35
4	910.28	15	57	9	19

The samples' <2  $\mu\text{m}$  fractions are generally dominated by illite with minor kaolinite and traces of chlorite with variable amounts of smectite. The invariance of the  $c.14\text{\AA}$  peak after K-saturation and heating to  $300^\circ\text{C}$ , coupled with its expansion after Ca-saturation and glycol-solvation indicate a lack of vermiculite in these samples.

Newmod-for-Windows<sup>TM</sup> modelling suggests that the illite in the Nordland Shale samples shows very restricted 'swelling' on glycol-solvation, exhibited by a slight sharpening of its basal XRD reflections, which may represent the presence of very few (<2%) smectite interlayers. Modelling indicates that the illite contains 0.7 K; 0.1 Fe per  $(\text{Si}, \text{Al})_4\text{O}_{10}(\text{OH})_2$  and typically a crystallite-size distribution with a mean defect-free distance of 8 layers and a crystallite-size range of 1 to 32 layers.

The coincidence of the kaolinite and chlorite basal XRD reflections makes accurate modelling of both species difficult. However, by careful measurement of the chlorite  $d_{003}$  and separated kaolinite  $d_{002}$  and chlorite  $d_{004}$  peaks, mean defect-free distances of 11 and 7 layers and crystallite-size ranges of 1 to 60 and 1 to 20 layers were assumed for the kaolinite and chlorite respectively. The intensity ratios for the chlorite basal XRD peaks also suggest that the chlorite present is an iron-rich variety.

The smectite identified in the samples has a mean defect-free distance of 2 layers and a crystallite-size range of 1 to 8 layers.

### 4.3 GEOCHEMISTRY

The results of XRF and REE analysis by ICP-MS are summarised in Tables 5 and 6 respectively.

**Table 5. Summary of geochemistry by X-ray fluorescence spectroscopy**

Core No.	%													
	SiO <sub>2</sub>	TiO <sub>2</sub>	Al <sub>2</sub> O <sub>3</sub>	Fe <sub>2</sub> O <sub>3</sub> t	Mn <sub>3</sub> O <sub>4</sub>	MgO	CaO	Na <sub>2</sub> O	K <sub>2</sub> O	P <sub>2</sub> O <sub>5</sub>	SO <sub>3</sub>	ZrO <sub>2</sub>	LOI	Total
1	52.13	0.87	18.10	7.89	0.10	2.66	1.79	1.29	5.46	0.18	0.2	0.02	9.00	99.81
2	59.79	0.95	16.92	5.15	0.06	1.73	1.35	1.43	3.95	0.11	0.2	0.04	7.58	99.40
4	58.00	0.82	15.88	6.06	0.08	2.38	2.66	1.36	3.99	0.13	0.4	0.02	7.94	99.83

Core No.	ppm											
	V	Cr	Co	Ni	Cu	Zn	As	Rb	Sr	Y	Ba	Pb
1	135	111	16	42	28	107	15	168	117	29	460	23
2	134	116	14	38	26	88	12	134	123	32	579	22
4	139	114	16	46	28	91	16	137	148	26	447	23

**Table 6. Summary of geochemistry by ICP-MS.**

Core No.	ppm																			
	Zr	Nb	La	Ce	Pr	Nd	Sm	Eu	Tb	Gd	Dy	Ho	Er	Tm	Yb	Lu	Hf	Ta	Th	U
1	182	19.5	47	102.3	11.4	43.4	7.77	1.47	0.98	5.93	5.73	1.13	3.20	0.46	3.06	0.46	4.99	1.29	15.4	4.6
2	269	23.1	44	97.3	10.9	41.0	7.87	1.37	0.99	6.01	5.95	1.23	3.39	0.51	3.17	0.48	7.13	1.51	14.6	4.1
4	197	15.4	39	81.6	9.3	34.9	6.47	1.33	0.84	5.00	5.03	0.97	2.74	0.41	2.57	0.40	5.44	1.02	12.0	3.2

Bar charts to compare the geochemistry of the three core samples are shown in Figure 9. Further plots are shown in Figure 10 to compare the geochemistry of the core samples with that of the North American Shale Composite (Gromet *et al.*, 1984).

#### 4.4 SURFACE AREA AND CATION EXCHANGE CAPACITY DETERMINATIONS

The surface area and CEC of the mudstone samples will be chiefly determined by the quantity and types of clay mineral present. Smectite, typically has a 2-ethoxyethanol surface area of 800 m<sup>2</sup>/g compared to other clay minerals which may reach 100 m<sup>2</sup>/g.

Typical CEC values for standard clay minerals include smectite 79-112 milliequivalents per 100g, illite 27 meq/100g and kaolinite 1.9-3.3 meq/100g (van Olphen & Fripiat, 1979).

The results of surface area and CEC determinations are shown in Table 5. Surface areas (68.2-89.4 m<sup>2</sup>/g) are relatively low for mudstones, reflecting the low proportion of smectite present. Similarly the CEC values are also low, generally very similar and within the range 11.5 to 11.9 meq/100g.

#### 4.5 TOTAL ORGANIC CARBON ANALYSIS

The results of TOC determinations are also shown in Table 7. Percentage TOC values are low for all the samples analysed with values ranging from 0.49 to 0.72%.

**Table 7. Summary of surface area, CEC and TOC determinations**

Core No.	Mean depth (m)	Surface area m <sup>2</sup> /g	CEC (meq/100 g)	TOC (%)
1	906.17	84.1	11.5	0.49
2	907.58	68.2	11.5	0.72
4	910.28	89.4	11.9	0.49

#### 4.6 PETROGRAPHIC ANALYSIS

##### 4.6.1 Core 1 (906.13 – 906.20 m)

This sample is a grey-green, soft, weakly laminated, silty mudstone with some drilling mud (predominantly KCl observed under the SEM) contamination lining the few hairline, subvertical fractures. The lamination is weakly defined by parallel-oriented muscovite and biotite flakes that float within a very fine-grained clay matrix.

The detrital grains are well sorted, medium to fine, predominantly fine, angular to subangular silt (Figure 11) and comprise quartz, K-feldspar, muscovite, biotite and calcite with trace foraminifera tests. Trace opaques include titanite and ilmenite as fine silt-sized grains. Insignificant and largely isolated secondary porosity develops through K-feldspar corrosion.

The clay matrix comprises submicron to micron-scale clay flakes welded together in a moderately to well-compacted fabric (Figure 12). Wispy, poorly developed authigenic illitic(?) overgrowths occur throughout. Moderate bioturbation or soft-sediment deformation is suggested by more random particle orientations with edge-to-edge contacts and an occasional domainal structure (e.g. Figure 21), although this is not observed in the core.

Trace primary porosity is infilled by several authigenic minerals. Isolated subhedral pyrite crystals up to 3  $\mu\text{m}$  across occur as a 'dusting' throughout the clay. Pyrite also forms lenses up to several millimetres across, parallel to primary lamination, that comprise clusters of well-developed framboids (e.g. Figure 19). Framboidal pyrite also develops within sheltered porosity of rare foraminifera and trace secondary porosity of occasionally altered muscovite and biotite, together with ankerite and rare sphalerite (e.g. Figure 13).

Dolomite is a minor authigenic component forming anhedral very fine silt-sized crystals typically with euhedral micron-scale manganoan ankerite overgrowths. Ankerite also occurs as isolated, micron-scale subhedral crystals throughout the matrix (Figure 12), which occasionally form larger patches of crystal aggregates up to 20-40 microns long, oriented parallel to the lamination. Both dolomite and ankerite were not detected by XRD analysis, almost certainly because they are present at levels below the XRD detection limit of *c.*0.5%. The clay matrix around framboidal pyrite clusters contains a slightly higher density of ankerite crystals, which, together with the close association with pyrite in sheltered and minor secondary porosity, suggests that pyrite and ankerite may be paragenetically associated.

#### **4.6.2 Core 2 (907.55 – 907.60 m)**

This sample is a grey-green, soft, moderately compacted silty mudstone. Occasional short, irregular lenses of silt to very fine sand occur parallel to the lamination. Well-sorted, detrital fine silt grains comprise subrounded to subangular quartz, K-feldspar, plagioclase, muscovite and biotite that float within the clay matrix (Figure 14). Rare and corroded foraminifera occur throughout. Opaques include Mn-rich ilmenite, rare zircons and pyroxene, which is typically altered. Rare fine sand-sized lithics, now composed of relict quartz only, are altered with trace dissolution porosity developed. Feldspars are irregular and corroded although any resultant secondary porosity around grain edges is infilled by clay matrix. The clay matrix comprises micron-scale irregular, welded flakes that define the weak lamination. In some areas clay forms domains of less-compacted clay, rounded aggregates or more irregularly oriented domains, suggesting bioturbation or soft-sediment deformation (Figure 21). Authigenic clay overgrowths were also observed which block pore-throats (Figure 22).

Both muscovite and biotite are altered with splaying along basal cleavages and precipitation of REE phosphates (Figure 15) plus rare ankerite (Figure 16) in the resulting insignificant secondary porosity. Note that large micas and chlorites are typically deformed through compaction that leads to replacement by kaolinite (Figure 17 and 18).

Unlike Core 1 (906.13 – 906.20 m), authigenic carbonate is not extensively developed in this sample. Only rarely is ankerite developed as a replacive phase in altered chlorite (Figure 16). Pyrite is also less extensive although occasionally forms lenses up to several millimetres across, parallel to primary lamination, that comprise clusters of well-developed framboids (Figure 19).

#### **4.6.3 Core 4 (910.26 – 910.30 m)**

This sample is a grey-green, weakly laminated, silty mudstone with well sorted angular to subrounded, fine silt sized detrital grains floating in a moderately to poorly compacted clay matrix. Detrital grains comprise angular to subrounded quartz, K-feldspar, plagioclase, muscovite and biotite that float within the clay matrix (Figure 20). Opaques include Mn-rich ilmenite, rutile, titanite, rare zircons and monazite, which is typically altered. Feldspars are irregular and corroded although any resultant secondary porosity around grain edges is infilled by clay matrix. Detrital phyllosilicate grains, especially chlorites, are commonly altered and partially replaced by kaolinite.

Authigenic carbonates include both dolomite and ankerite as isolated, very fine-grained, sub-micron crystals within the clay matrix. Coarser, fine –silt-sized anhedral, angular detrital dolomite grains also act as seeds for partially developed ankerite overgrowths.

The clay matrix comprises micron-scale irregular welded illitic flakes that define the weak lamination. In some areas clay forms domains of less-compacted clay, rounded aggregates or more irregularly oriented domains, suggesting bioturbation or soft-sediment deformation or sedimentation as silt-sized clay pellets (Figure 21). Each domain is around 10-50  $\mu\text{m}$  in diameter i.e. of comparable size to the silt grains. Authigenic clay overgrowths are suggested blocking pore-throats (Figure 22). Authigenic pyrite is rare and limited to framboidal aggregates.

## 5 Discussion

### 5.1 COMPARISON WITH PREVIOUS STUDIES

The three cores samples of Nordland Shale from this study are composed of fine-grained clays or silty clays that share broadly similar characteristics to the cuttings samples studied by Lingren *et al.* (2002), Kemp *et al.* (2001), Bøe & Zweigel (2000) and Lothe & Zweigel (1999). In most respects, the shallowest core (Core 1) appears to be slightly different to the apparently similar Cores 2 and 4.

Core 1 is classified as a clay compared to the slightly coarser-grained Cores 2 and 4 which represent silty clays. Cuttings examined by Lingren *et al.* (2002) from the Sleipner and Ekofisk areas and those studied by Kemp *et al.* (2001) from UK Quadrant 16 were also predominantly classified as silty clays. Since the core samples contain 33% silt-grade material and show a weak sedimentary lamination, they may also be classified as clayshales according to Lundegard & Samuels (1980). This differs from the descriptors 'mudshales' where laminated or 'mudstones' where massive attributed to the samples examined by Kemp *et al.* (2001).

The TOC contents of the core samples are low, ranging from 0.49 to 0.72% and similar to those obtained by Kemp *et al.* (2001) which ranged 0.68 to 1.58%. This means that the core samples can be further classified as non-organic clayshales (Krushin, 1997).

The deeper Cores 2 and 4 have an average composition of undifferentiated mica (42%), quartz (30%), kaolinite (7%), K-feldspar (7%), calcite (2%), smectite (2%), albite (8%), chlorite (<1%), pyrite (1%), halite (1%). Such a mineralogy appears more micaceous but generally concurs with previous analyses of the Nordland Shale from the UK Quadrant 16 (Kemp *et al.*, 2001). The shallower core from this study has a generally similar mineralogy to the deeper samples but due to its finer-grained nature it shows a greater proportion of clay minerals (e.g. 'mica' 60%, kaolin 10%) and a lesser proportion of minerals associated with silt-grade detrital material (e.g. quartz and feldspar). The shallow core also contains a greater proportion of minerals associated with the drying of saline porewater e.g. halite and sylvite. The fractured nature of Core 1 (Figure 3) may have introduced a greater proportion of drilling fluid into this sample than into the intact Cores 2 and 4. No evidence was obtained in this study or that of Kemp *et al.* (2001) for the presence of siderite, amphibole or zeolite identified by Bøe & Zweigel (2000). Petrographic examination did however identify the presence of dolomite and ankerite as minor authigenic components not detected by XRD analysis.

A lack of previously obtained geochemical data for Nordland Shale precludes comparison. Nevertheless, the XRF major element geochemistry is in broad agreement with the whole-rock mineralogy determined by XRD analysis and again indicates that Core 1 is slightly different to the more similar Cores 2 and 4. The  $\text{SiO}_2$  content of the cores, although contributed by quartz, feldspars and clay minerals, appears to follow the quartz concentration most closely.  $\text{Al}_2\text{O}_3$  and  $\text{K}_2\text{O}$  contents and loss on ignition figures are greatest in Core 1, reflecting the greater 'mica' content of this sample. However, the XRF-determined  $\text{Fe}_2\text{O}_3$  content of the cores is greater than would be expected from the XRD-determined pyrite and chlorite concentrations. This may

suggest the presence of poorly-crystalline Fe-oxyhydroxide species in the cores that were not detected by XRD analysis or specifically identified by SEM analysis.

The trace and rare earth geochemistry of the core samples is also similar with only minor differences related to the identified changes in mineralogy. For example Core 1 shows higher Rb and REE concentrations than the other samples which is probably related to its higher clay and particularly 'mica' content. Rb commonly substitutes for K in micas. The relatively high Sr content of Core 4 reflects its higher calcite content, since Sr is known to substitute for Ca in calcite. The higher Ba and Zr contents of Core 2 probably reflect the increased concentration of barite and zircon respectively.

The geochemistry of the core samples is generally similar to that of the NASC (Figure 10). The Nordland Shale appears to be relatively depleted in Ca and As but enriched in Na, presumably due to halite precipitation from saline water intrusion. REE show a very similar distribution to the NASC with a very slight enrichment in LREE.

The <2 µm clay mineralogy of the core samples is predominantly composed of illite (average 55%), kaolinite (27%), chlorite (10%) and smectite (8%). Again this concurs with the shallower samples (above *c.*3400 ft) examined by Kemp *et al.* (2001). These authors found that deeper samples were characterised by increased smectite and kaolinite contents such as illite 41%, kaolinite 37% and smectite 23% in the deepest sample (3839 ft). Bøe & Zweigel (2000) identified a similar increase in smectite beneath a shallower depth of 675 m (2215 ft) in well N 15/9-9. The low levels of smectite present in the core samples from the present study appears to correspond with a position some 100 m above the Utsira Formation. Lingren *et al.* (2002) found an approximately uniform clay mineralogy from three Sleipner wells of smectite, vermiculite, illite and kaolinite but made no attempt to quantify these phases. No evidence was found for the presence of vermiculite in the present study.

Consistent CEC values of *c.*12 meq/100g and surface areas of *c.*80 m<sup>2</sup>/g provide further evidence for the presence of small quantities of smectite. The clay mineral assemblage and their relatively small crystallite size distributions obtained from Newmod-modelling suggests that they have only reached the Early Diagenetic grade of maturity (Merriman & Kemp, 1996) and have undergone only shallow burial of perhaps 1-2 km.

Scanning electron microscopy of the core samples revealed many of the features described by Kemp *et al.* (2001). The core samples have a weak, sedimentary lamination defined by the parallel orientation of mica flakes which occasionally shows evidence of bioturbation. The small proportions of fine sand- and silt-grade detrital grains are predominantly composed of quartz, K-feldspar and calcite with some rare bioclastic debris. The clay matrix is composed of submicron to micron-scale clay flakes welded into a moderately to well-compacted fabric. Primary and secondary porosity are very limited and often infilled by authigenic framboidal pyrite, dolomite and ankerite. The lack of porosity and evidence for advanced diagenetic processes provides further confirmation for the shallow burial of the Nordland Shale.

## 5.2 SEAL CAPACITY PREDICTION

Krushin (1997) suggested it is possible to predict the seal capacity of a non-smectitic, non-organic shale from its displacement pore throat diameter which in turn is related to its mineralogy and in particular its quartz content. In a study of mature Precambrian- to Jurassic-aged shales, he found that greater quartz contents produced larger pore throat sizes (assumed for this study to be diameters) and therefore lower seal capacities. By employing his equation:

$$\text{displacement pore throat diameter (nm)} = 1.4(\% \text{quartz in matrix}) - 20.5$$

XRD-determined quartz contents for the present study suggest displacement pore throat diameters of 2.2, 23.5 and 21.1 nm for Cores 1, 2 and 4 respectively. On this basis, the lower quartz content of Core 1 results in a predicted pore throat diameter an order of magnitude lower than those predicted for Cores 2 and 4. However, since the largest pore throats measured in smectite-rich shales are regarded as drying-artefacts, Krushin (1997) was unable to validate his relationship between displacement pore throat diameter and quartz content by mercury injection porosimetry (MIP) for more immature shales. Although the Nordland Shale samples of the present study are essentially non-organic (0.49 to 0.72% TOC), they contain trace amounts (<2%) of smectite. It is therefore questionable whether such 'trace amounts' of smectite render the Krushin (1997) method of seal capacity determination inapplicable to the Nordland Shale.

Using the simplifications of Lindberg (1997), it is then possible to relate the displacement pore throat radius ( $r$  in nm) to the required pressure difference ( $\Delta p$  in MPa) for CO<sub>2</sub> to enter a water wet shale pore where  $\sigma$  (in mN/m) is the surface tension between water and CO<sub>2</sub>:

$$\Delta p = \frac{2\sigma}{r}$$

Assuming the surface tension of CO<sub>2</sub> to be as low as 20 mN/m, as it is likely to be close to its critical point in the case of the Sleipner injection, and displacement pore throat radii of 1.1, 11.7 and 10.5 nm, capillary entry pressures of 36.7, 3.4 and 3.8 MPa respectively are predicted.

According to Bøe & Zweigel (2000), the density difference between CO<sub>2</sub> and water at reservoir conditions of  $c.300 \text{ kg/m}^3$  creates a buoyancy pressure of 0.003 MPa for a 1 m thick CO<sub>2</sub> column. Therefore, the predicted capillary entry pressures suggest that the Nordland Shale, represented by these core samples is capable of trapping a CO<sub>2</sub> column ranging from 11469, 1063 and 1188 m high. Bøe & Zweigel (2000) obtained similar results for the Nordland Shale in Norwegian Quadrant 15, predicting that a 860 m high CO<sub>2</sub> column could be trapped and that cap rock capillary leakage was unlikely to occur. Kemp *et al.* (2001) obtained a range of displacement pore throat radii from 7.25 to 20 nm, capillary entry pressures of 2 to 5.5 MPa and predicted that the Nordland Shale in the UK Quadrant 16 could support a CO<sub>2</sub> column ranging from 667 to 1833 m high. Since the Utsira Sand has a maximum thickness of  $c.300 \text{ m}$  in the Sleipner area, capillary leakage through the Nordland Shale would therefore appear unlikely.

## 6 Conclusions

- The three cores samples of Nordland Shale from well 15/9-A-11 show broadly similar characteristics to previously studied cuttings. The shallowest core sample (Core 1, 906.17 m) appears slightly different to the more similar, deeper cores (Core 2, 907.58 m and Core 4, 910.28 m).
- The cores are composed of fine-grained clays or silty clays and are classified as non-organic clayshales using the Krushin (1997) criteria.
- The deeper samples (Cores 2 and 4) have an average composition of undifferentiated mica (42%), quartz (30%), kaolinite (7%), K-feldspar (7%), calcite (2%), smectite (2%), albite (8%), chlorite (<1%), pyrite (1%), halite (1%). Core 1 is finer-grained and contains a greater proportion of clay minerals (e.g. 'mica' 60%, kaolin 10%) and a lesser proportion of minerals associated with silt-grade detrital material (e.g. quartz and feldspar).
- The cores have a weak, sedimentary lamination defined by the parallel orientation of mica flakes which occasionally shows evidence of bioturbation. Primary and secondary porosity is limited and often infilled by authigenic framboidal pyrite, dolomite and ankerite.
- The clay matrix is composed of submicron to micron-scale clay flakes welded into a moderately to well-compacted fabric and composed of illite (average 55%), kaolinite (27%), chlorite (10%) and smectite (8%). The low levels of smectite present in the core samples, indicated by XRD, CEC and surface area analysis, appears consistent with a sample location, *c.*100 m above the Utsira Formation and is indicative of shallow burial of perhaps 1-2 km. The lack of porosity and evidence for advanced diagenetic processes provides further confirmation for the shallow burial of the Nordland Shale.
- Little variation was found in the major, trace and rare earth element geochemistry of the Nordland Shale samples which appears very similar to the North American Shale Composite (NASC). Geochemical variations can generally be explained in terms of the detected mineralogy with the exception of  $\text{Fe}_2\text{O}_3$  which may suggest the undetected presence of poorly crystalline Fe-oxyhydroxides.
- Although small quantities of smectite in the Nordland Shale may invalidate its predictions, XRD-determined quartz contents suggest displacement pore throat diameters of 2.2, 23.5 and 21.1 nm for Cores 1, 2 and 4 respectively using the Krushin (1997) methodology. Such displacement pore throat diameters predict capillary entry pressures of between 3.8 and 36.7 MPa and are capable of trapping a  $\text{CO}_2$  column ranging from 1063 to 11469 m high. As concluded in previous studies, considering that the Utsira Sand has a maximum thickness of *c.*300 m in the Sleipner area, capillary leakage through the Nordland Shale would appear unlikely.

## References

Most of the references listed below are held in the Library of the British Geological Survey at Keyworth, Nottingham. Copies of the references may be purchased from the Library subject to the current copyright legislation.

- BØE, R, and ZWEIGEL, P. 2001. Characterisation of the Nordland Shale in the Sleipner area by XRD analysis - A contribution to the Saline Aquifer CO<sub>2</sub> Storage (SACS) project. *SINTEF Petroleum Research Report No. 33.0764.00/01/01*
- CARTER, D L, HEILMEN, M D and GONZALEZ, F L. 1965. Ethylene glycol monoethyl ether for determining surface area of silicate minerals. *Soil Science* **100**, 356-360.
- CHADWICK, R A, HOLLOWAY, S, KIRBY, G A, GREGERSON, U and JOHANNESSEN, P N. 2000. The Utsira Sand, Central North Sea – an assessment of its potential for regional CO<sub>2</sub> disposal. *Proceedings of the 5th International Conference on Greenhouse Gas Control Technologies (GHGT-5)*, Cairns, Australia, 349 – 354.
- GROMET, L.P., DYMEK, R.F., HASKIN, L.A., and KOROTEV, R. L. 1984. The "North American shale composite"; its compilation, major and trace element characteristics. *Geochimica et Cosmochimica Acta*, **48**, 2469-2482.
- HALLSWORTH, C R, and KNOX, R W O'B. 1999. BGS Rock Classification Scheme. Volume 3. Classification of sediments and sedimentary rocks. *British Geological Survey Research Report*, RR 99–03.
- HILLIER, S. 1999. Use of an airbrush to spray dry samples for X-ray powder diffraction. *Clay Minerals*, **34**, 127-135.
- HILLIER, S., SUZUKI, K. and COTTER-HOWELLS, J. 2001. Quantitative determination of Cerussite (lead carbonate) by X-ray powder diffraction and inferences for lead speciation and transport in stream sediments from a former lead mining area of Scotland. *Applied Geochemistry*, **16**, 597-608.
- KEMP, S.J., BOUCH, J. and MURPHY, H.M. 2001. Mineralogical characterisation of the Nordland Shale, UK Quadrant 16, northern North Sea. *British Geological Survey Commissioned Report*, CR/01/136.
- KRUSHIN, J T. 1997. Seal capacity of nonsmectite shale. 31-47 in *Seals, Traps and the Petroleum System*. SURDAM, R C (editor). AAPG Memoir 67.
- LINDBERG, E. 1997. Escape of CO<sub>2</sub> from aquifers. *Energy Convers. Mgmt.*, **38**, Supp., S235-S240.
- LINGREN, H, FRIES, K and SPRINGER, N. 2002. SACS, Task 1.4: Evaluation of cap rock sealing the reservoir. Clay mineralogy investigation of core and cuttings from the Ekofisk and Sleipner areas. *GEUS Confidential Report*.
- LOTHE, A E, and ZWEIGEL, P. 1999. Saline Aquifer CO<sub>2</sub> Storage (SACS). Informal annual report 1999 of SINTEF Petroleum Research's results in work area 1 'Reservoir Geology'. *SINTEF Petroleum Research Report No. 23.4300.00/03/99*
- LUNDEGARD, P M and SAMUELS, N D. 1980. Field classification of fine-grained sedimentary rocks. *Journal of Sedimentary Petrology*, **50**, 781-786.
- MERRIMAN, R J and KEMP, S J. 1996. Clay minerals and sedimentary basin maturity. *Mineralogical Society Bulletin*, **111**, 7-8.
- MOORE, D M and REYNOLDS, R C. 1997. *X-Ray Diffraction and the Identification and Analysis of Clay Minerals*, Second Edition. Oxford University Press, New York.
- REYNOLDS, R C and REYNOLDS, R C. 1996. *Description of Newmod-for-Windows™. The calculation of one-dimensional X-ray diffraction patterns of mixed layered clay minerals*. R C Reynolds, 8 Brook Road, Hanover, NH 03755, USA.
- SHEPARD, F P. 1954. Nomenclature based on sand-silt-clay ratios. *Journal of Sedimentary Petrology*, **24**, 151-158.
- SNYDER, R.L. and BISH, D.L. 1989. Quantitative analysis. In: Bish, D.L., Post, J.E. (Eds), *Modern Powder Diffraction*, Reviews in Mineralogy, Volume 20, Mineralogical Society of America, USA, pp. 101-144 (Chapter 5).
- VAN OLPHEN, H and FRIPIAT, J J. 1979. *Data handbook for Clay Materials and other Non-Metallic Minerals*. Pergamon Press.

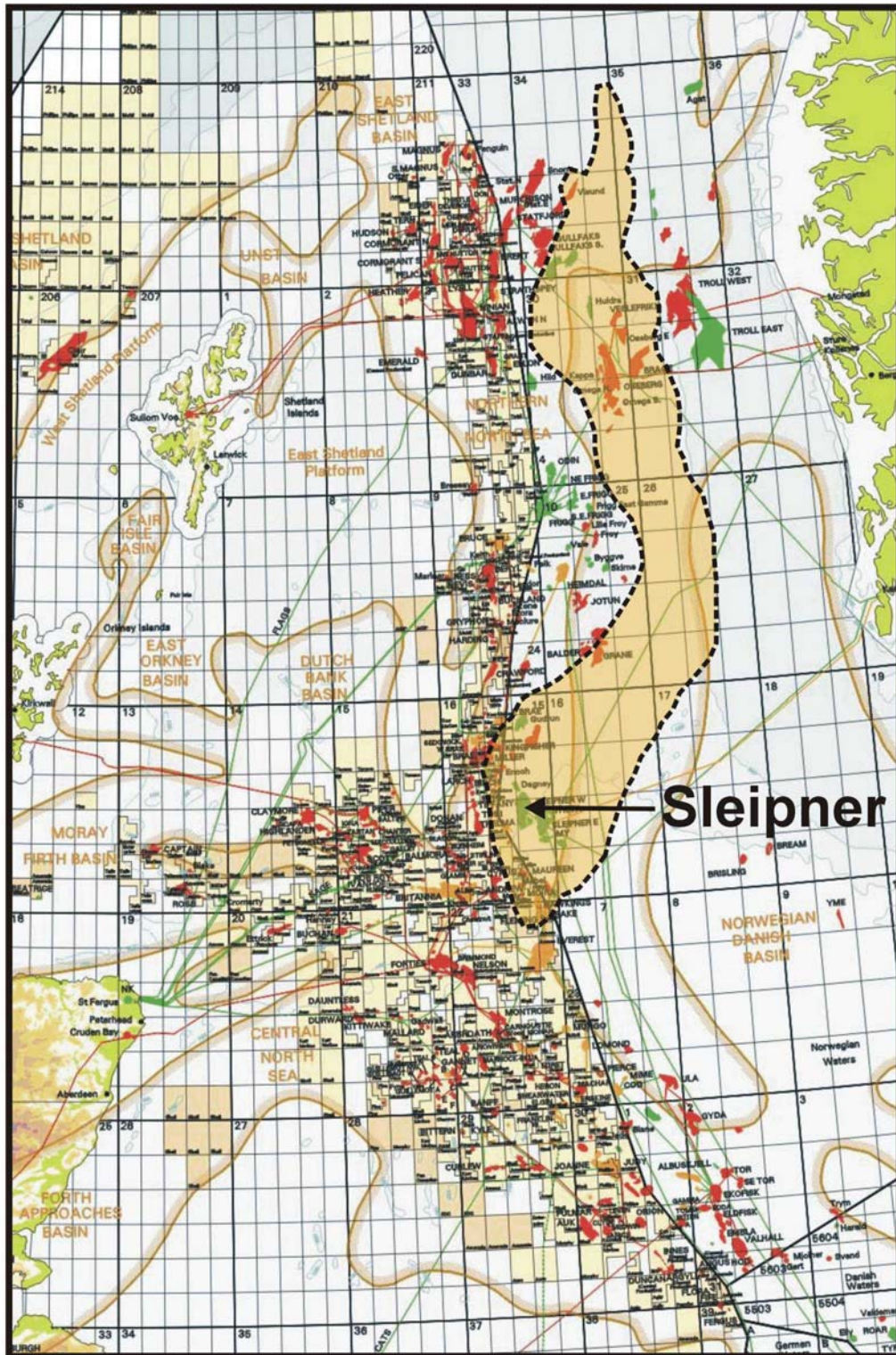


Figure 1. Northern and Central North Sea map showing location of the Sleipner field.

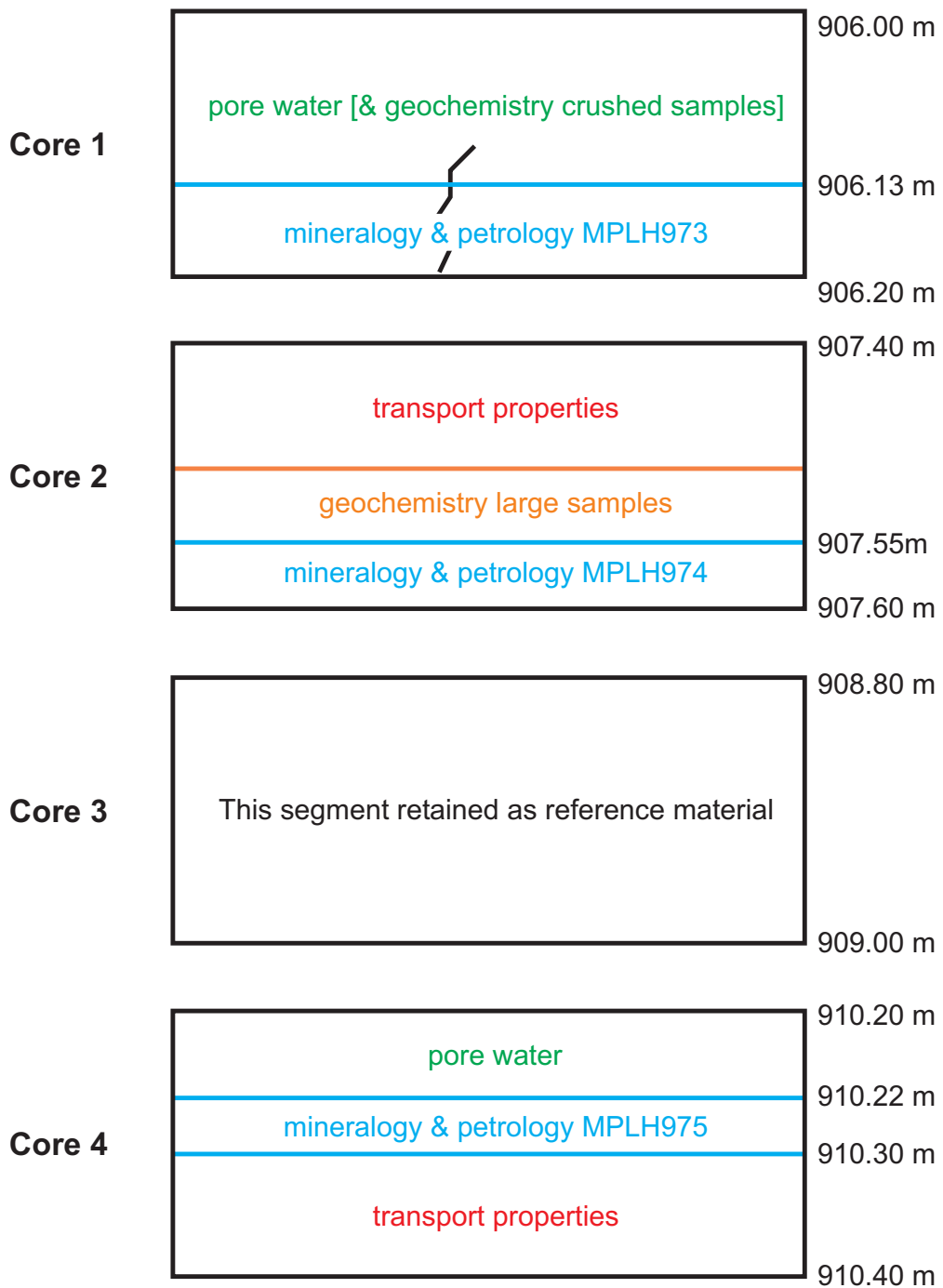
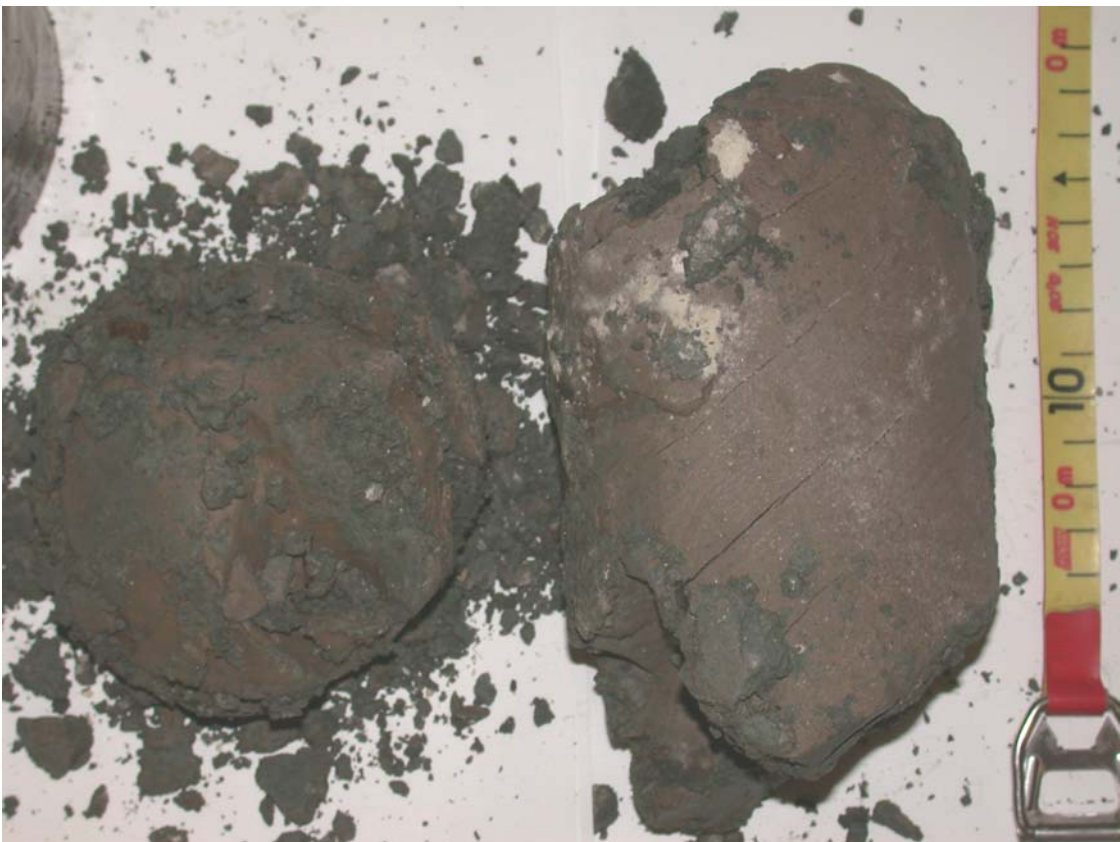


Figure 2. BGS sampling strategy for the four Sleipner caprock cores



**Figure 3. Core 1, 906.13 – 906.20 m, end-view prior to liner removal (above), side-view following liner removal (below).**



**Figure 4. Core 2, 907.55 – 907.60 m, end-view prior to liner removal (above), side-view following liner removal (below).**



**Figure 5. Core 4, 910.22 – 910.30 m, end-view prior to liner removal (above), side-view following liner removal (below).**

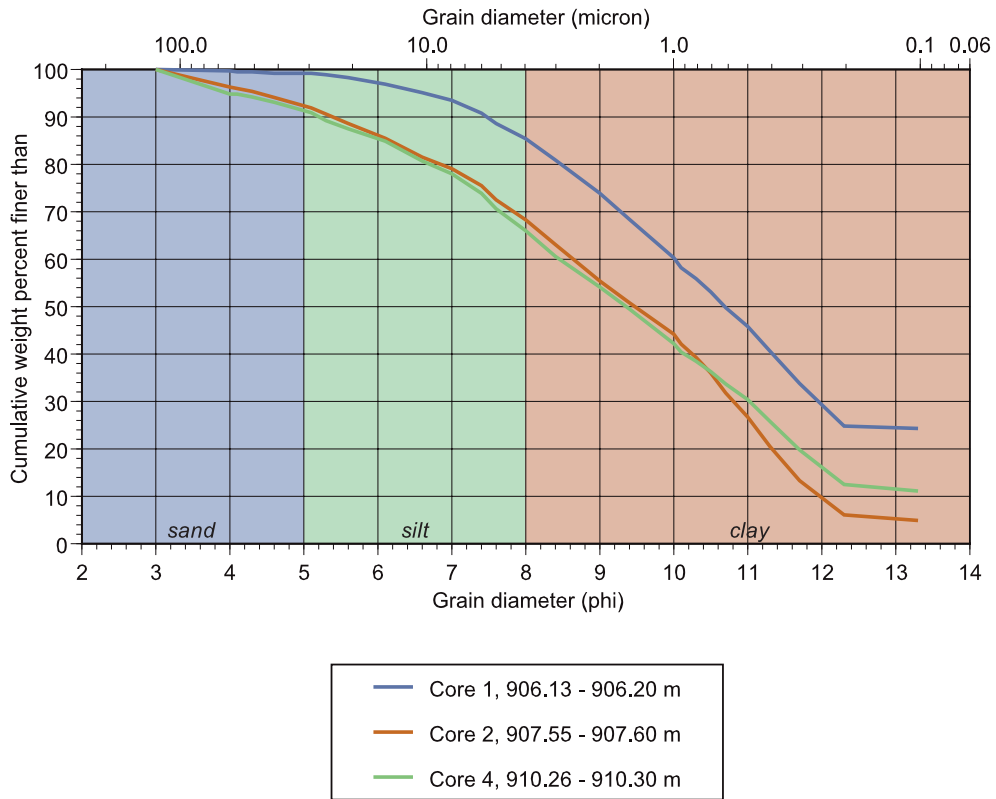


Figure 6. Cumulative plot of particle-size data.

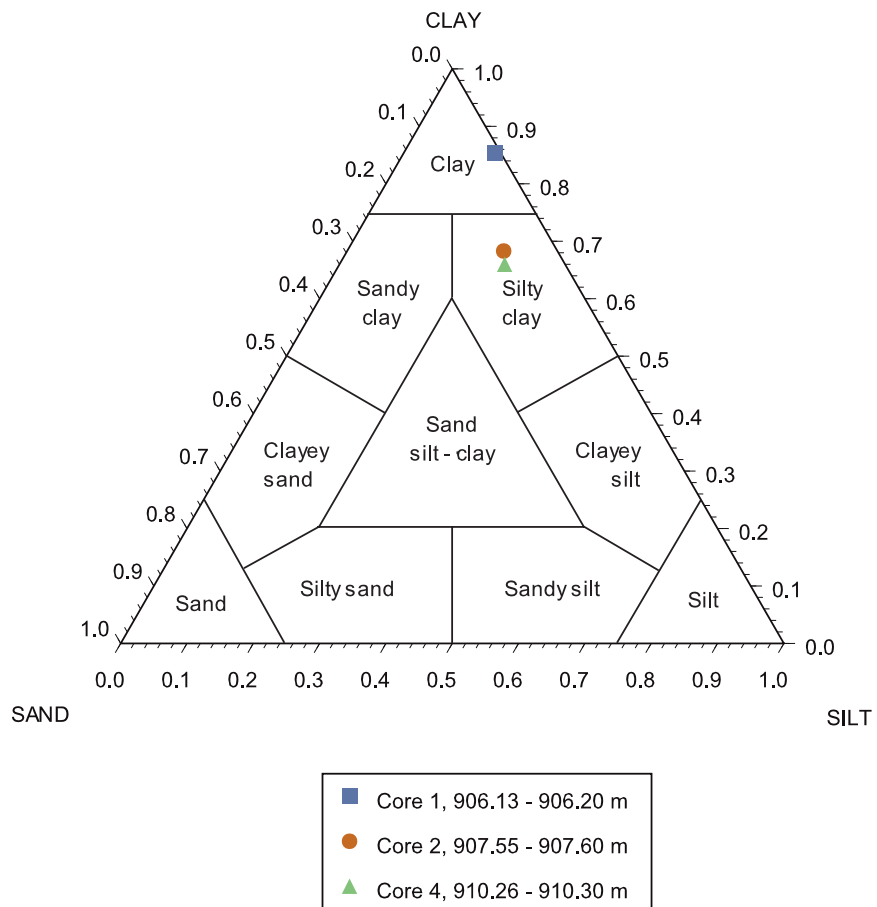
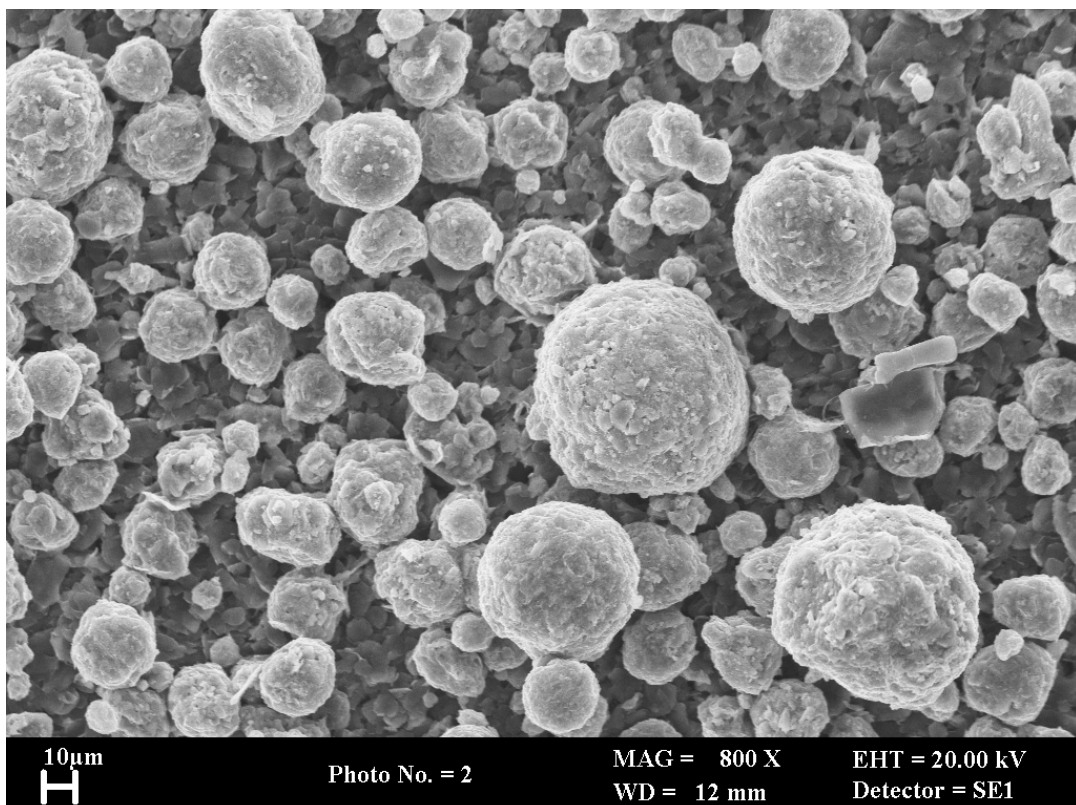
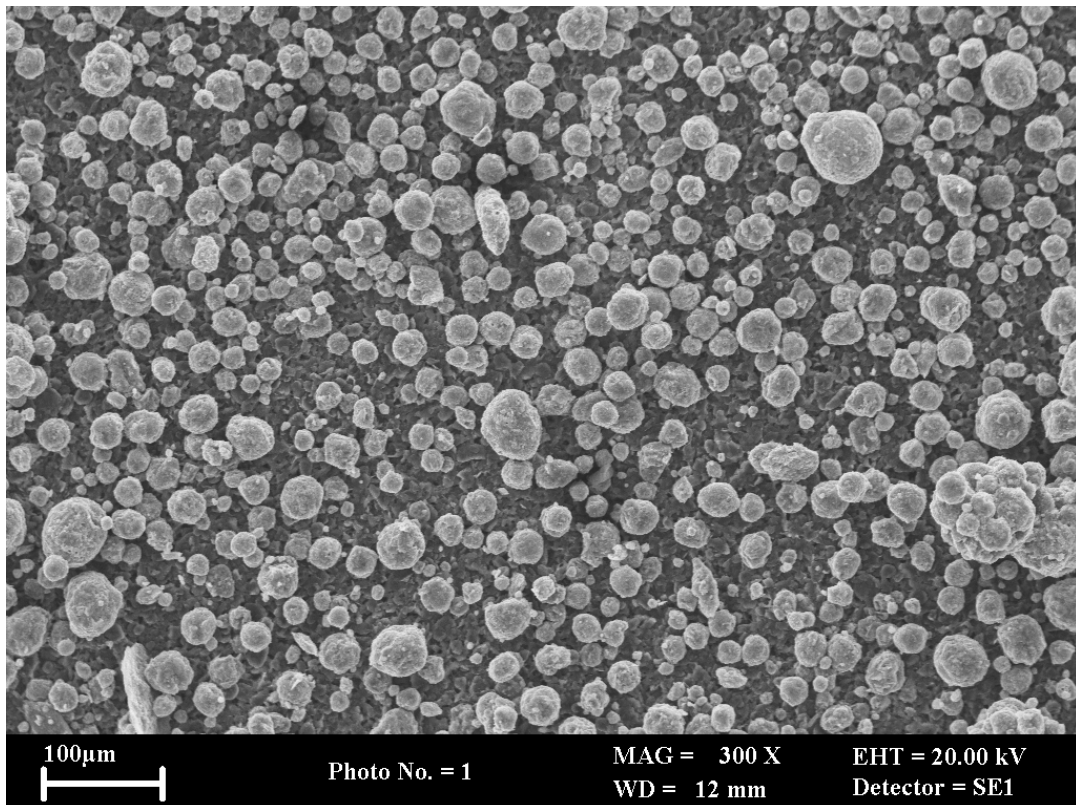


Figure 7. Triangular plot of particle-size data (after Shepard, 1954)



**Figure 8. Scanning electron photomicrographs of spherical granules produced by spray-drying to ensure a random arrangement of component particles for whole-rock XRD analysis, sample Core 1, 906.13 – 906.20 m.**

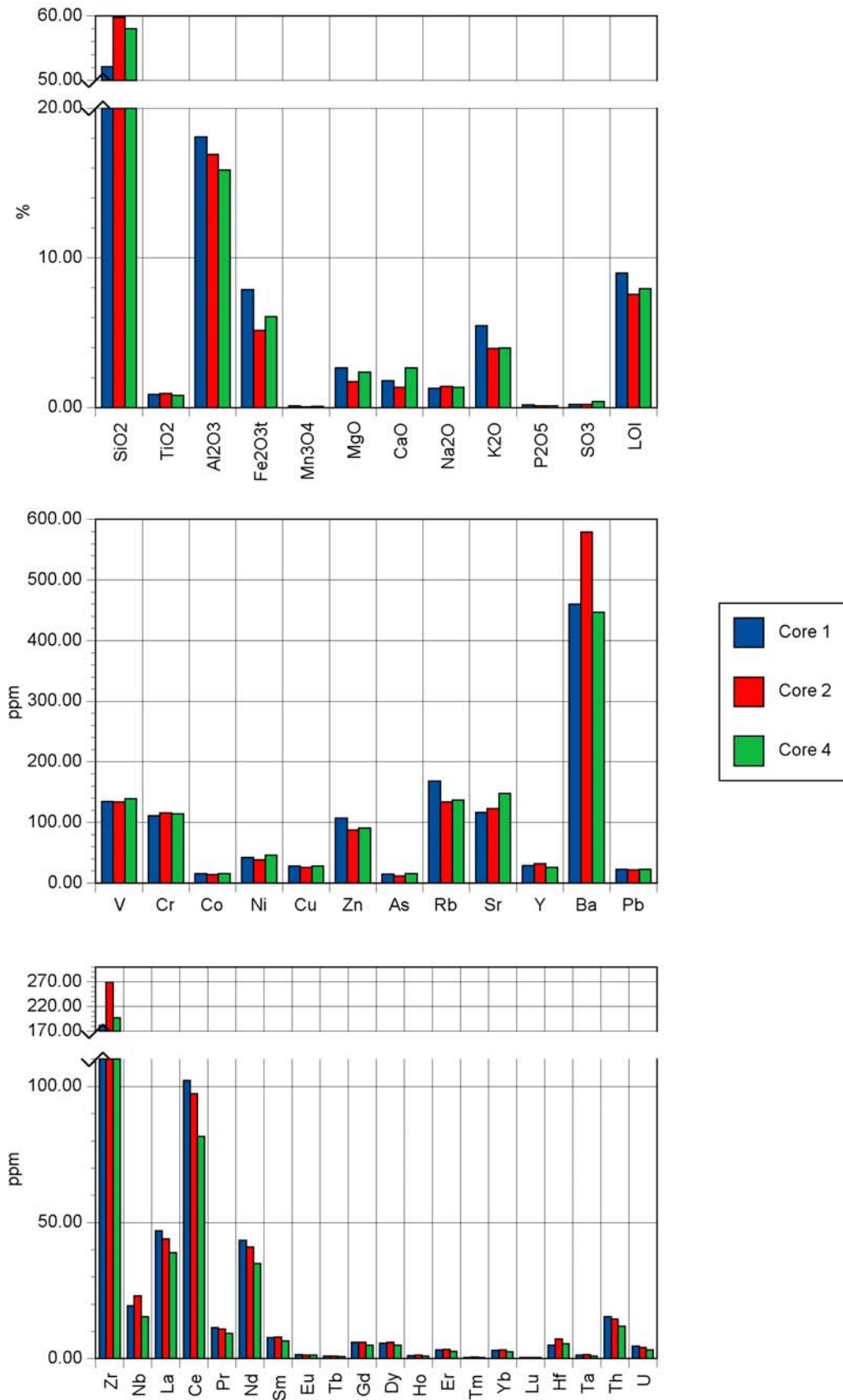


Figure 9. Geochemistry of the core samples, XRF major elements (upper chart), selected XRF trace elements (middle chart) and ICP-MS trace elements (lower chart).

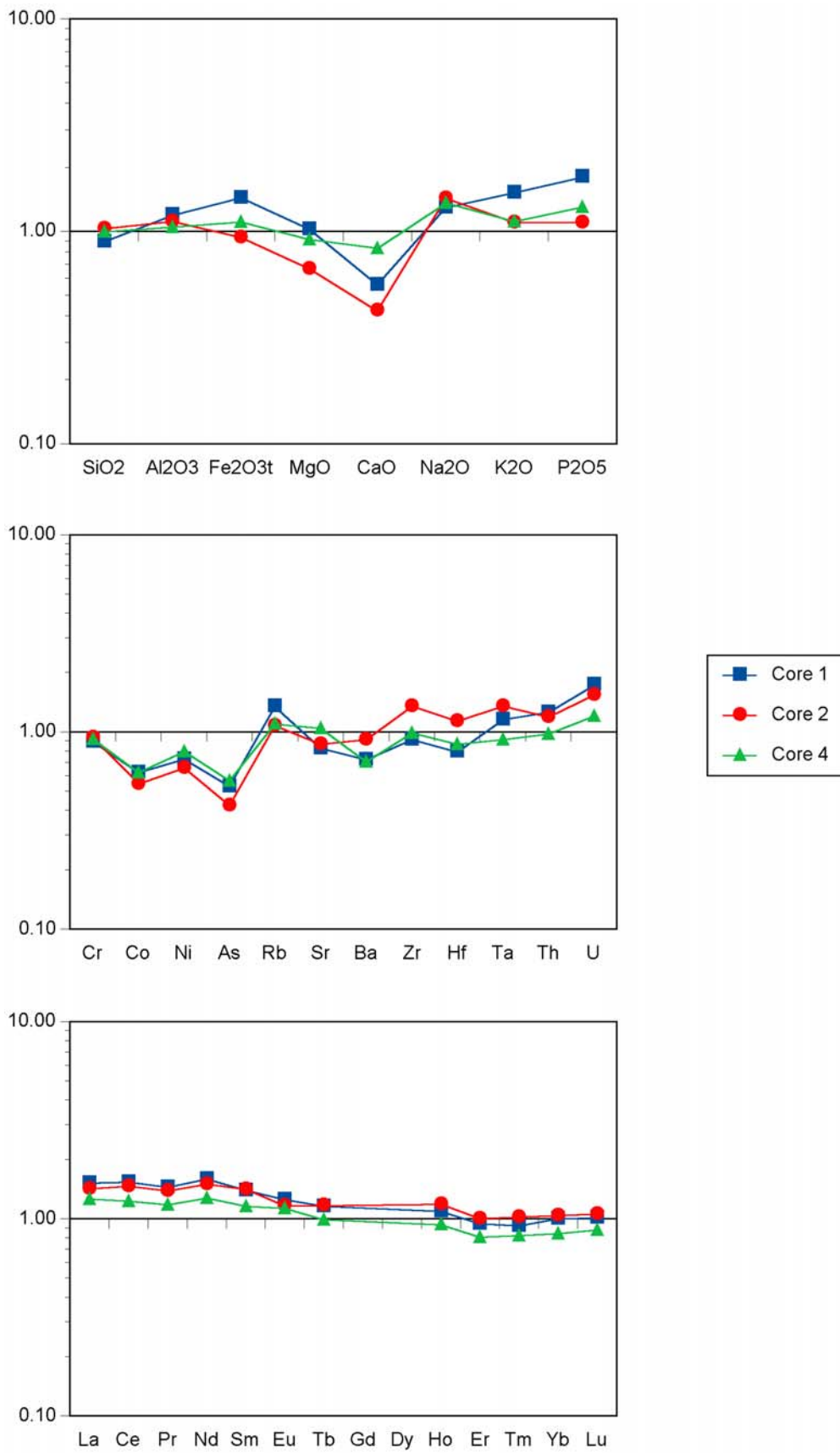


Figure 10. Geochemical distributions for the core samples compared to the North American Shale Composite (Gromet *et al.*, 1984).

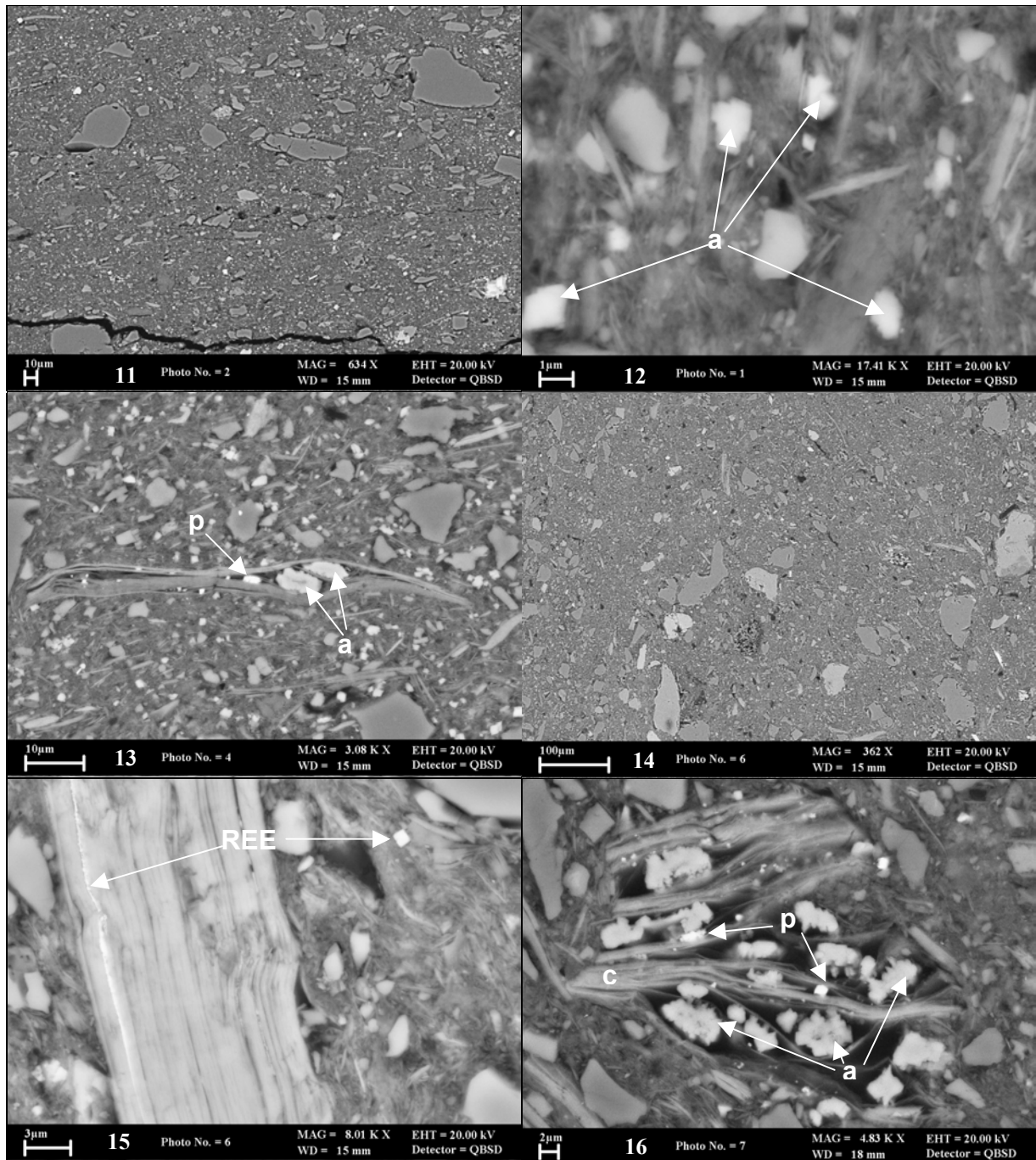


Figure 11. Typical, weakly laminated, moderately compacted silty mudstone comprising medium-sized subangular silt grains in a clay matrix. Core 1 (906.13 – 906.20 m). H973P101.tif.

Figure 12. Detailed view of typical moderately compacted clay fabric with very fine detrital silt grains and authigenic ankerite (a) occurring throughout. Core 1 (906.13 – 906.20 m). H973P102.tif.

Figure 13. A detrital, altered muscovite grain with ankerite (a) and pyrite (p) infilling secondary porosity along basal cleavages. Note moderate compaction and mica alignment around coarser silt grains. Core 1 (906.13 – 906.20 m). H973P104.tif.

Figure 14. Typical view of silty mudstone from Core 2 (907.55 – 907.60 m). Note irregular silt grains, and partially replaced phyllosilicates. H974P106.tif.

Figure 15. A biotite grain which is altering and splaying along basal cleavages, within which REE-phosphates (REE) are precipitating. Note rare authigenic REE-phosphate (REE) close-by in the matrix. Core 2 (907.55 – 907.60 m). H974P101.tif.

Figure 16. A rare, severely altered chlorite (c) with ankerite (a) and pyrite (p) precipitating in resultant secondary porosity. Core 2 (907.55 – 907.60 m). H974P107.tif.

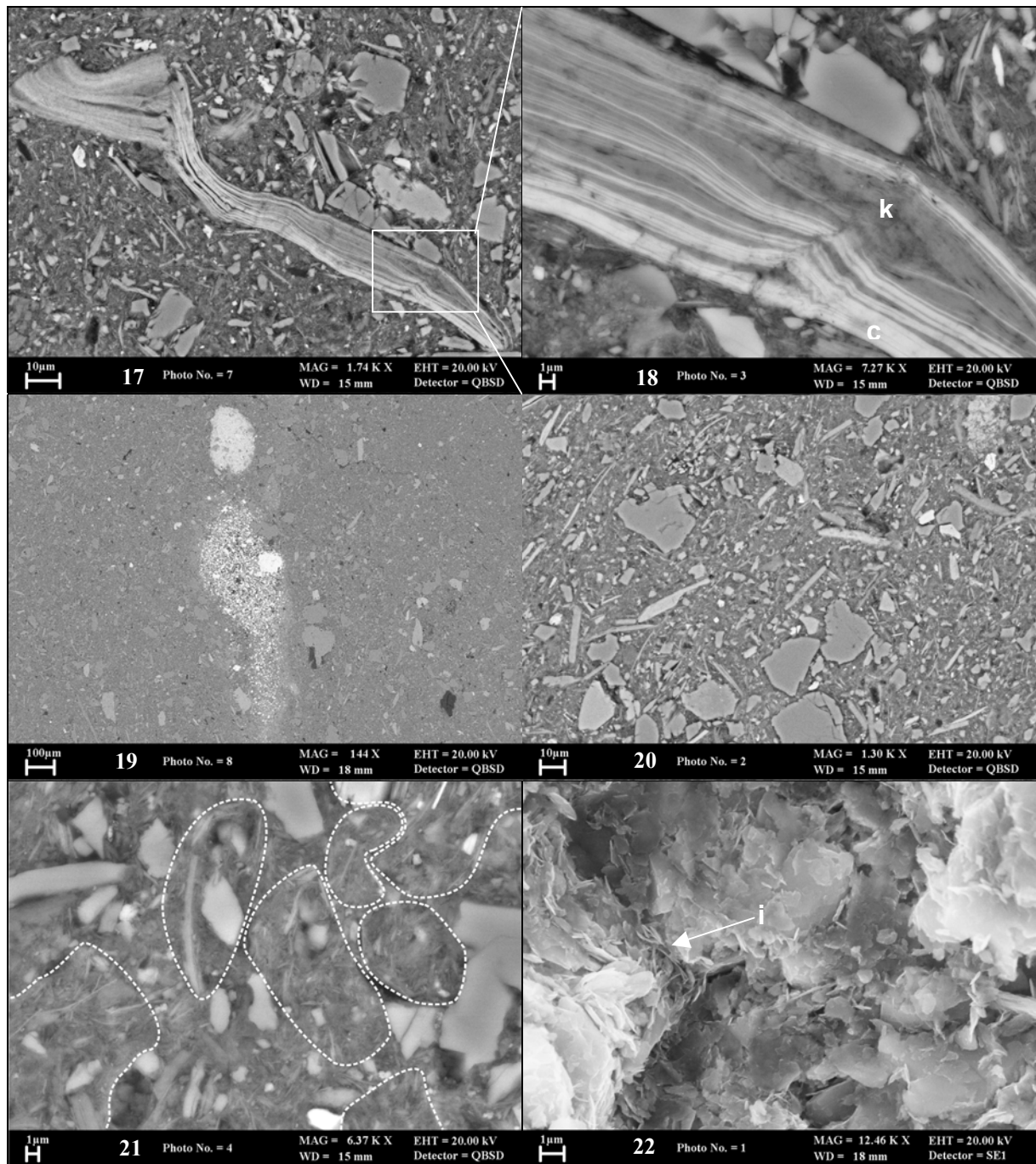


Figure 17. A detrital and compactionally deformed chlorite flake that is being replaced by kaolinite. Core 2 (907.55 – 907.60 m). H974P102.tif.

Figure 18. A close-up of the altered chlorite (c) in Figure 13, being replaced by kaolinite (k). Core 2 (907.55 – 907.60 m). H974P103.tif.

Figure 19. Framboidal pyrite aggregates forming millimetre-scale lenses. Core 2 (907.55 – 907.60 m). H974P108.tif.

Figure 20. Typical view of moderately compacted silty mudstone with lamination defined by parallel oriented detrital phyllosilicates, from Core 4 (910.26 – 910.30 m). H975P102.tif.

Figure 21. Detailed view of domainal orientations, identified by dashed boundaries, in the clay matrix. Core 4 (910.26 – 910.30 m). H975P103.tif.

Figure 22. A silt grain plucked during specimen preparation reveals pore-throats blocked by detrital and authigenic illitic clay flakes (i). Core 4 (910.26 – 910.30 m). H975S101.tif.

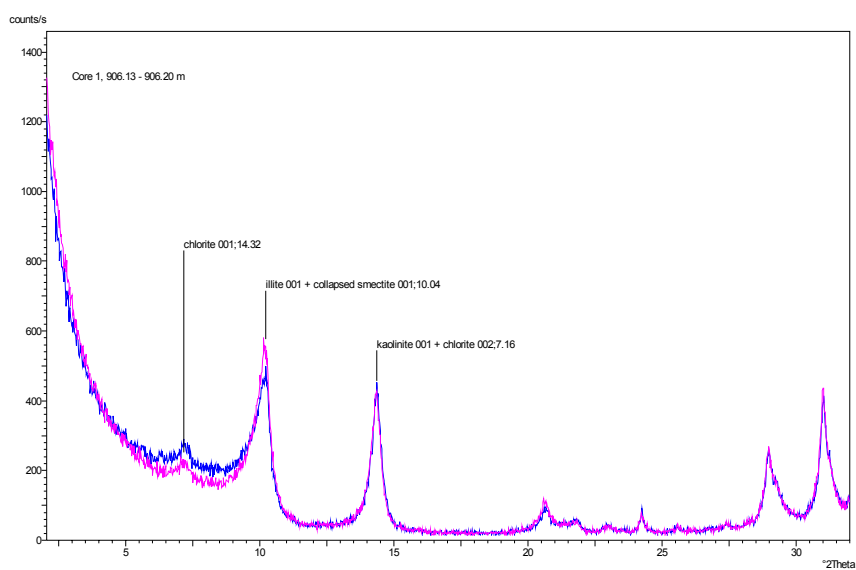
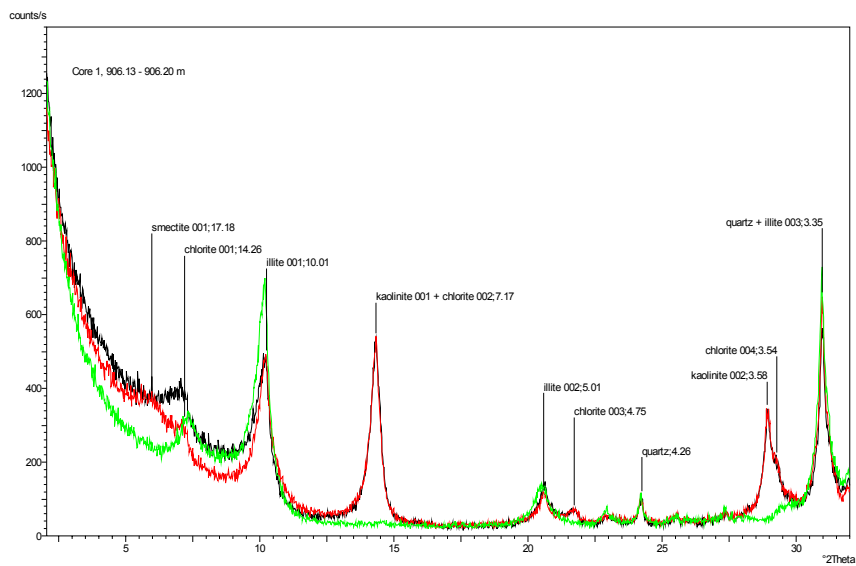
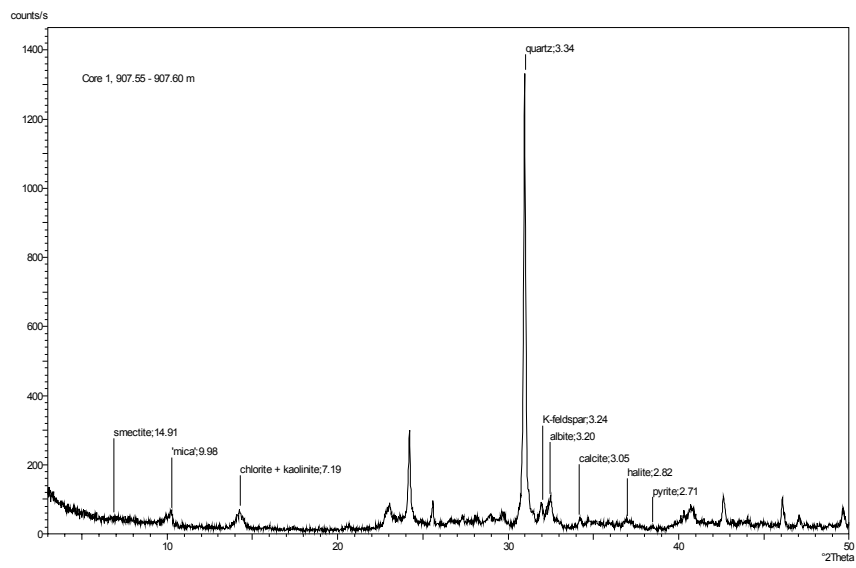


## Appendix - X-ray diffraction traces

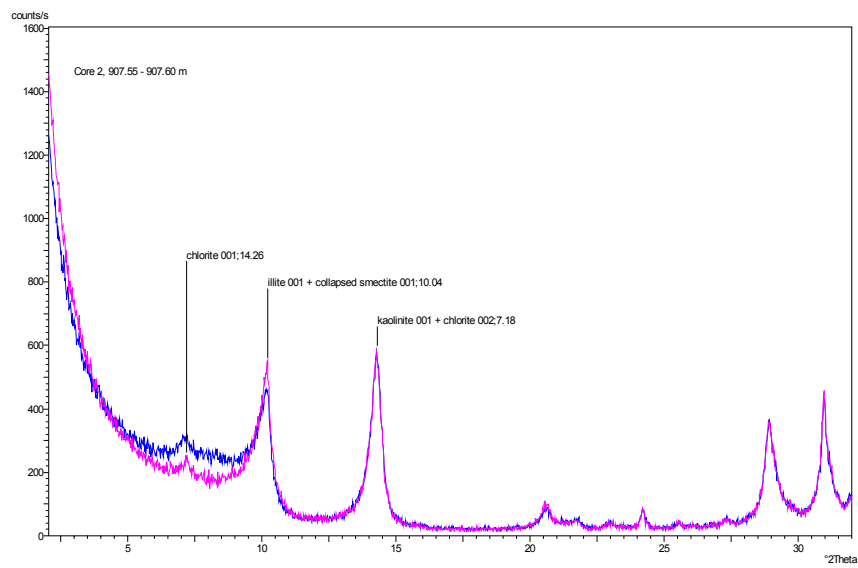
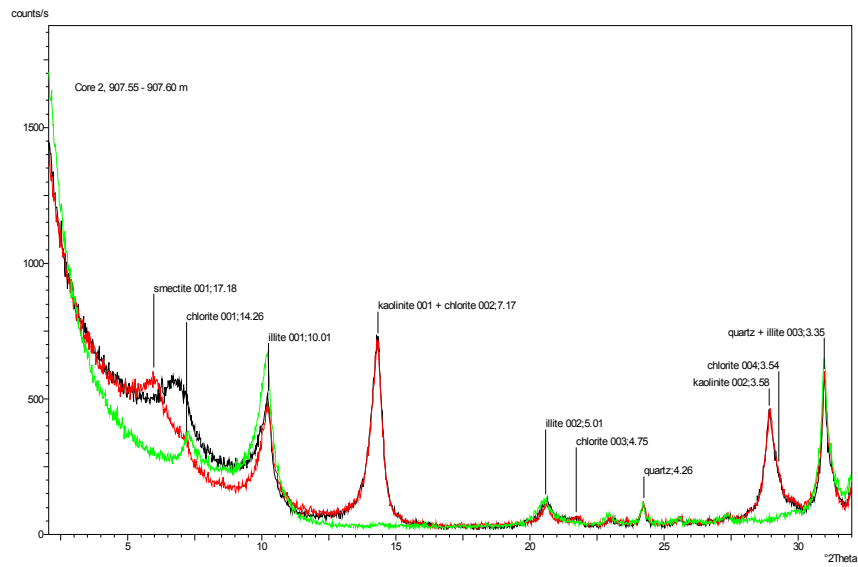
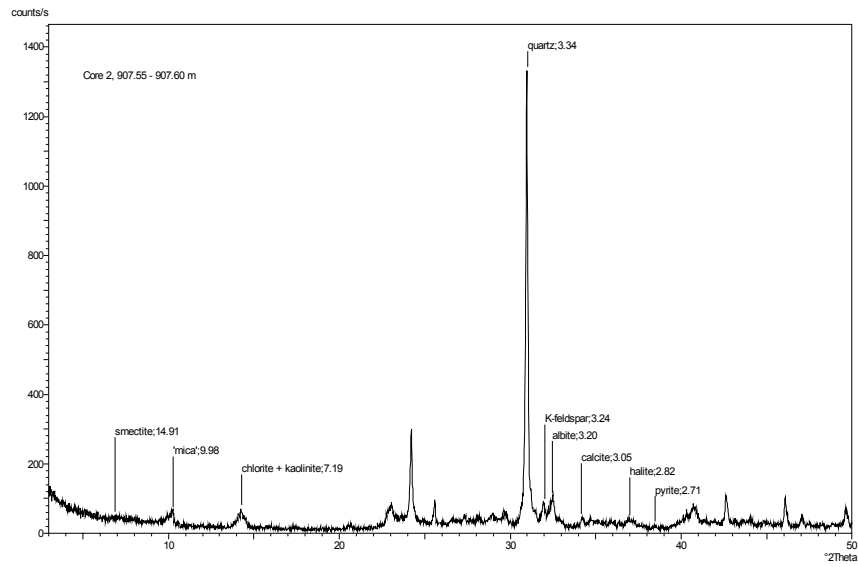
In each case, a whole-rock trace is shown uppermost with the Ca-saturated <2  $\mu\text{m}$  fraction oriented mount traces centre (air-dry; black trace, glycol-solvated; red trace, heated 550°C/2 hours; green trace) and the K-saturated <2  $\mu\text{m}$  fraction oriented mount traces lowermost (air-dry; blue trace, heated 300°C/2 hours; magenta trace).

Horizontal scales show  $^{\circ}2\theta$  Co-K $\alpha$  while vertical scales show intensity in counts/second. For the whole-rock traces, diagnostic peaks are labelled for each identified mineral phase including its d spacing ( $\text{\AA}$ ). All peaks are labelled for the Ca-saturated <2  $\mu\text{m}$  fraction glycol-solvated traces including the miller index (00*l*) for the clay minerals. Diagnostic peaks are labelled for the K-saturated <2  $\mu\text{m}$  fraction heated traces including the miller index (00*l*) for the clay minerals.

### Core 1, 906.13 – 906.20 m



### Core 2, 907.55 – 907.60 m



### Core 4, 910.26 – 910.30 m

